Interfacial Structure Dependent Spin Mixing Conductance in Cobalt Thin Films

M. Tokaç,[1,*] S. A. Bunyaev,[2] G. N. Kakazei,[2] D. S. Schmool,[3] D. Atkinson,[1] and A. T. Hindmarch[1,†]
[1]Centre for Materials Physics, Durham University, South Road, Durham DH1 3LE, United Kingdom
[2]IFIMUP and IN, Departamento de Física e Astronomia, Universidade do Porto, 4169-007 Porto, Portugal
[3]Laboratorie PROMES CNRS (UPR 8521), Université de Perpignan Via Domitia, Rambla de la Termodynamique, Tecnosud, 66100 Perpignan, France

(Received 18 March 2015; revised manuscript received 6 May 2015; published 30 July 2015)

Enhancement of Gilbert damping in polycrystalline cobalt thin-film multilayers of various thicknesses, overlayered with copper or iridium, was studied in order to understand the role of local interface structure in spin pumping. X-ray diffraction indicates that cobalt films less than 6 nm thick have strong fcc(111) texture while thicker films are dominated by hcp(0001) structure. The intrinsic damping for cobalt thicknesses above 6 nm is weakly dependent on cobalt thickness for both overlayer materials, and below 6 nm the iridium overlayers show higher damping enhancement compared to copper overlayers, as expected due to spin pumping. The interfacial spin mixing conductance is significantly enhanced in structures where both cobalt and iridium have fcc(111) structure in comparison to those where the cobalt layer has subtly different hcp(0001) texture at the interface.

DOI: 10.1103/PhysRevLett.115.056601 PACS numbers: 72.25.Mk, 75.70.Cn, 76.50.+g

A quantitative physical analysis of spin currents crossing interfaces [1–3] in ferromagnetic (FM) thin-film multilayers will provide a deeper fundamental understanding required for applications of such nanoscale magnetic systems in magnonics [4], spin caloritronics [5,6], and spintronics [7–9]. Precessional magnetization dynamics have been used extensively to access interfacial spin transport where spin current flows from magnetization precession in a FM thin film into an adjacent nonmagnetic (NM) layer. This spin current is then dissipated under the influence of the spin-orbit interaction (SOI) resulting in an enhanced damping in the FM layer [10], a process known as spin pumping [11,12].

In conventional spin-pumping theory [12,13] the relaxation of a spin current in the NM layer is parametrized by the spin-mixing conductance $g_{\uparrow\downarrow}$, which has generally been assumed to be solely a property of the NM material. However, a recent theoretical study by Liu *et al.* developed a more complex picture of spin pumping [2], which explains the experimentally observed damping enhancements for various material combinations [14]. In this model the "effective" mixing conductance $g^{\mathrm{eff}}_{\uparrow\downarrow}$ contains terms that quantify not only relaxation of the spin current within the NM layer $g_{\uparrow\downarrow}$, but also the ability of the spin current to cross the FM-NM interface, characterized by an effective specific interface spin resistance R^* and relaxation associated with crossing the interface, termed spin memory loss δ. Chen and Zhang very recently proposed an alternate model, based on spin memory loss due to interfacial (Rashba, in their calculations) SOI [1]. Because of interfacial spin resistance and/or spin memory loss, details of the FM-NM interface structure can have an important role in determining the damping contribution due to spin pumping [6,9].

This Letter describes the results of spin-pumping measurements using a more complex multilayered sample structure with FM (Co) sandwiched between NM layers in symmetric (Ta/Cu underlayers and Cu/Ta overlayers) and asymmetric (Ta/Cu underlayers, Ir/Ta overlayers) structures to demonstrate the role of local interface structure in spin pumping. Cobalt and iridium are isoelectronic, and Ir has strong SOI. Figure 1 shows a schematic of the structures and possible spin currents. Provided the spin current can traverse the interface from the FM to the $\mathrm{NM}_1^{L,R}$ layers (as anticipated for Co/Cu and Co/Ir interfaces), the precession of the magnetization in FM, $M(t)$, generates a spin current $J^{L,R}_{\mathrm{s\,pump}}$ from the FM layer into both adjacent NM layers, providing two parallel channels for energy dissipation. In steady state this pumped spin current may relax within the $\mathrm{NM}_1^{L,R}$ layers, it may generate spin accumulation in $\mathrm{NM}_1^{L,R}$, which would then cause a backflow of spin current into the FM layer as $J_{s1}^{L,R}$, and/or it may reach the outer $\mathrm{NM}_2^{L,R}$ layers as $J_{s2}^{L,R}$ [13].

For Ta/Cu underlayers and Cu/Ta overlayers, the $\mathrm{NM}_1^{L,R}$ (Cu) layers are much thinner than the spin diffusion

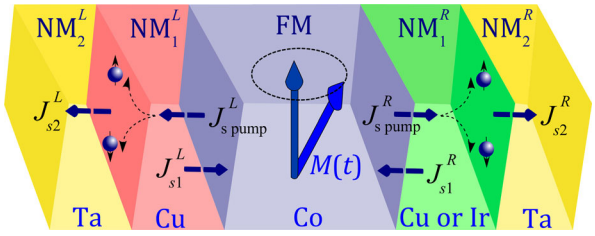

FIG. 1 (color online). A schematic of the sample structures used in this study, and examples of possible spin currents generated by spin pumping.

length so spin mixing in these layers should be negligible. The effective specific interface resistance between $NM_1^{L,R}$ and $NM_2^{L,R}$ (Ta) should be high [2,14], so it is expected that $J_{s2}^{L,R} \sim 0$, and the spin backflow $J_{s1}^{L,R} \approx J_{s\,\mathrm{pump}}^{L,R}$; thus, the damping enhancement should be negligible. However, for Ir/Ta overlayers, when NM_1^R (Ir) is thicker than the spin diffusion length, $J_{s\,\mathrm{pump}}^R$ may fully relax within NM_1^R; now $J_{s1}^R \approx 0$, again $J_{s2}^R \sim 0$, and the damping should be enhanced.

By studying the FM thickness dependence of ferromagnetic resonance (FMR) in symmetric and asymmetric polycrystalline multilayer structures, it is shown here how the dynamic magnetization behavior depends intricately upon the crystal structure of the FM layer and how the precessional damping is influenced by both the NM overlayer and the local interfacial structure. This allows the spin-pumping contributions to the damping from individual interfaces, with different local atomic-scale structures, to be determined.

Two series of films were fabricated onto thermally oxidized Si substrates by dc and rf magnetron sputtering at deposition rates of ~ 0.02 nm/s^{-1} in an Ar atmosphere using an ultrahigh vacuum deposition system. The layer structures were Si/SiO/Ta/Cu/Co[t_{Co}]/Cu (or Ir)/Ta with a Co thickness t_{Co} ranging from 2.5 to 55 nm. The thicknesses of the other metal layers was fixed at 3 nm. The samples showed in-plane magnetization for all t_{Co}. The crystallographic properties were investigated by XRD with Cu-$K\alpha$ radiation. Layer thicknesses and interfacial roughnesses (0.3 ± 0.1 nm for all interfaces in all samples studied) were determined from fitting x-ray reflectivity using GENX software [15].

FMR measurements were carried out at room temperature using a coplanar waveguide (CPW) connected to a vector network analyzer. A dc magnetic field was applied along the axis of the CPW. The samples were placed film down on the CPW, and the complex S_{21} parameter [example shown in the inset of Fig. 3(a)] was measured as a function of the external magnetic field over a frequency range up to 18 GHz. The FMR frequency f and linewidth ΔH were extracted from the raw data as described in Ref. [16]. The FMR condition for a FM thin film can be described by the Kittel formula [17],

$$f = \frac{\gamma}{2\pi}\sqrt{H_{\mathrm{res}}(H_{\mathrm{res}} + 4\pi M_{\mathrm{eff}})}, \tag{1}$$

where H_{res} is the applied magnetic field at resonance and $\gamma = g\mu_B/\hbar$ is the gyromagnetic ratio which is proportional to g, the Landé (g) factor. For a continuous polycrystalline film of thickness t_{FM}, the effective demagnetization field is

$$4\pi M_{\mathrm{eff}} = 4\pi M_S + \frac{2K_S}{M_S t_{\mathrm{FM}}}, \tag{2}$$

with M_S is the saturation magnetization and K_S is the perpendicular surface magnetic anisotropy constant [18].

The effective magnetization was determined by fitting the frequency dependence of the resonance field using Eq. (1), as shown in the inset of Fig. 2(a). The inverse Co thickness dependence of the effective demagnetization field for both Cu and Ir overlayered film series is shown in Fig 2(a). For structures with the same Co thickness but different overlayers, $4\pi M_{\mathrm{eff}}$ has the same value, which demonstrates that Cu and Ir overlayers do not significantly influence the anisotropy field, as found previously for Pt/Co/Ir [19]. It is clear that the data in Fig. 2(a) are not described well by Eq. (2); instead, the data are divided into thin and thick film regions and each region was analyzed independently using Eq. (2). There is a clear thickness dependence of $4\pi M_{\mathrm{eff}}$ in each thickness regime, decreasing linearly with increasing inverse Co thickness, indicating that these variations are an interfacial effect, as assumed in Eq. (2). The dashed line is the best fit to films with $t_{\mathrm{Co}} \leq 6$ nm and the solid line is a fit to the thicker films. Extracted values for M_S and K_S are given in Table I, and are comparable to those found elsewhere [20–22].

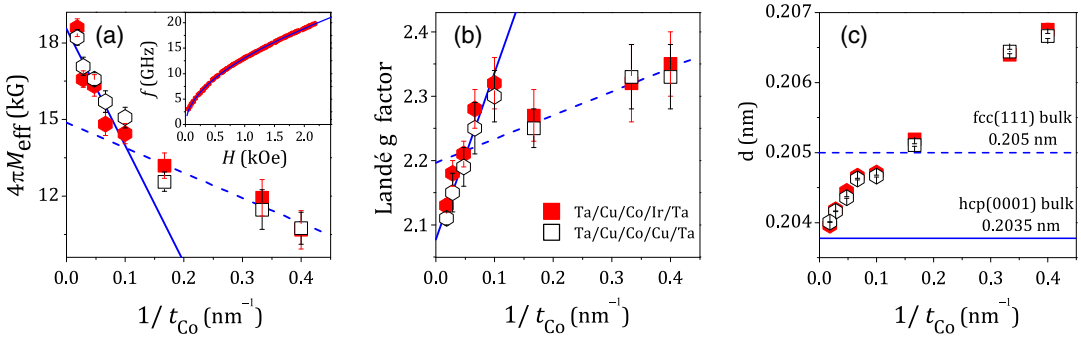

FIG. 2 (color online). (a) Inverse Co thickness dependence of the effective demagnetization field. The inset shows an example of resonance frequency as a function of magnetic field for the Co[55 nm]/Ir sample and a fit to the Kittel formula. (b) Inverse Co thickness dependence of the Landé g factor. In (a) and (b) the solid (dashed) lines are representative linear fits to thicknesses greater (less) than 6 nm. (c) Inverse Co layer thickness dependence of the interplanar spacing of Co for the Cu- and Ir-overlayered film series, extracted from XRD measurements. Squares and hexagons represent dominant fcc(111) and hcp(0001) texture in the Co layer, respectively.

TABLE I. Parameters extracted from spin-pumping measurements (saturation magnetization, M_S; surface magnetic anisotropy constant, K_S; bulk Landé g factor, g_{bulk}; bulk Gilbert damping, α_0; and effective spin-mixing conductance, $g_{\uparrow\downarrow}^{\text{eff}}$), showing comparison with relevant literature values. The literature value for K_S quoted for comparison from Ref. [23] is taken as negative due to a difference in sign convention.

Spin-pumped interface(s)	M_S (emu/cm^3)	K_S (erg/cm^2)	g_{bulk}	$\alpha_0(\times 10^{-3})$	$g_{\uparrow\downarrow}^{\text{eff}}$ ($\times 10^{18}$ m^{-2})
hcp(0001)-Co/Cu/Ta	1470 ± 40	-2.8 ± 0.4	2.07 ± 0.01	(7.1 ± 0.2)	(0.4 ± 0.1)
fcc(111)-Co/Cu/Ta	1100 ± 100	-0.42 ± 0.05	2.19 ± 0.02	(5.5 ± 0.3)	(1.8 ± 0.1)
hcp(0001)-Co/Ir/Ta	1470 ± 60	-3.3 ± 0.5	2.09 ± 0.01	(7.5 ± 0.2)	(0.6 ± 0.1)
fcc(111)-Co/Ir/Ta	1200 ± 200	-0.56 ± 0.06	2.21 ± 0.02	(5.2 ± 0.3)	(9.1 ± 0.5)
Co/Pt (quoted from Ref. [3])					80
Ta/Cu/Co/Cu/Pt (Ref. [23])	1456	-1.04	2.15	8.5	7.3
Pt/Cu/Co/Cu/Pt (Ref. [21])	1131	-0.46 ± 0.04	2.49 ± 0.14		0.89 ± 0.12

The Landé g factor was also determined from γ values extracted from fitting Eq. (2), and is shown in Fig. 2(b). The data are clearly not independent of thickness, contrary to the common assumption [21]. Again, after splitting the samples into two thickness regimes, linear dependencies on $1/t_{\text{Co}}$ are observed, indicative of interface effects with slightly different behavior for thinner and thicker films. For both Cu and Ir overlayered films the g factor was larger than for bulk Co and decreases slightly with increasing t_{Co} in both thickness regimes. From the intercepts of the linear fits, bulk g factors, g_{bulk}, were estimated; these are also given in Table I, and are similar to values found elsewhere [21,24]. The g factor can be thought of as relating spin (μ_S) and orbital (μ_L) components of the atomic magnetic moment, where $g = 2 + 2(\mu_L/\mu_S)$. In the bulk, μ_L is largely quenched, but this quenching may be reduced at the interfaces where the crystal symmetry is broken. A slight increase in μ_L due to reduced quenching of angular momentum at the interfaces would enhance the g factor, which explains the linear decrease in the g factor as the inverse Co layer thickness decreases, as seen in Fig. 2(b). It is interesting to note that there is no clear correlation between the g factor, via enhanced μ_L, and K_S. Both $4\pi M_{\text{eff}}$ and the Landé g factor show that there is a significant difference between thicker and thinner films.

In order to investigate the reason for this difference, XRD measurements of the Cu- and Ir-overlayered series were used to determine the interplanar spacing d shown in Fig. 2(c). As the Co thickness increases, the interplanar spacing shifts to lower values, indicating that the crystallographic structure changes with increasing film thickness. Previous studies of Co/Cu multilayers have shown that for $t_{\text{Co}} < 4$ nm, a fcc Co structure is stable and a mixture of fcc and the hcp phases occurs in thicker layers [25]. Here the data also suggest that the initial growth of polycrystalline Co films is a predominantly (initially strained) fcc(111) phase and that as the film thickness increases beyond $t_{\text{Co}} \sim 6$ nm hcp stacking faults occur and a dominant hcp (0001) bulklike structure develops. It is to be noted that lattice mismatch between Co and Ir (~8%) [26] is larger compared to Co and Cu (~1.8%) [27].

The fcc(111) lattice structure consists of an *ABCABC* layer-stacking sequence, and the hcp(0001) lattice structure has *ABAB* stacking sequence; hcp stacking faults thus consist of a displacement of atomic planes from *C* to *A* sites. These hcp stacking faults contribute only to the inhomogeneous linewidth broadening (see Supplemental Material [28]). Cu and Ir overlayers are expected to have fcc(111) structure [26] for all Co thicknesses with a small (Co-layer thickness dependent) lattice strain. In all plots shown, Co films with predominantly fcc(111) and hcp(0001) texture are indicated by square and hexagonal symbols, respectively; this attribution is supported by the FMR data, particularly the Landé g factor. The combined thickness and crystal structure dependence of the g factor, as explained here, has not previously been considered.

The intrinsic magnetic damping α was extracted [16] from

$$\Delta H = \Delta H_0 + \frac{4\pi\alpha}{|\gamma|} f.$$

The intrinsic damping under the influence of spin pumping is related to the total effective spin-mixing conductance for the multilayer structure $g_{\uparrow\downarrow}^{T,\text{eff}}$ by [2,13,29]

$$\alpha = \alpha_0 + \frac{g\mu_B}{4\pi M_s t_{\text{FM}}} g_{\uparrow\downarrow}^{T,\text{eff}}, \tag{3}$$

where α_0 is the bulk intrinsic damping. The dependence of the intrinsic damping on the inverse Co thickness is shown in Fig. 3, with linear fits to Eq. (3) for each overlayer and dominant Co crystal-phase combination. The solid lines correspond to the (thicker) films with hcp(0001)-dominated structure and the dashed lines are fits to the (thinner) fcc(111)-dominated phase for Cu and Ir overlayered films. The α_0 were extracted from the intercepts, and are shown in Table I; these agree well with literature values for bulk hcp Co [30], and a recent theoretical prediction for bulk fcc Co [29].

In principle, the slope of the fits shown in Fig. 3 allow us also to extract $g_{\uparrow\downarrow}^{T,\text{eff}}$ for fcc(111)- and hcp(0001)-dominated phases, and Cu and Ir overlayered films. It is clear that $g_{\uparrow\downarrow}^{T,\text{eff}}$

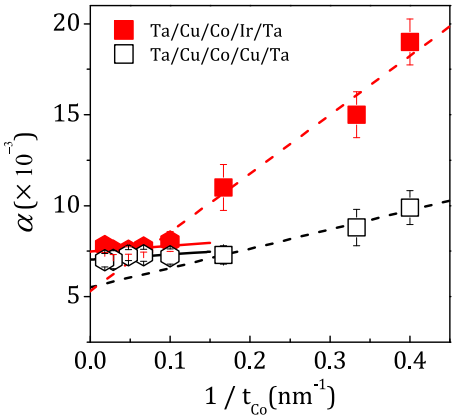

FIG. 3 (color online). The inverse Co thickness dependence of the Gilbert damping parameter α for both sets of films. The solid and dashed lines are linear fits to the structures with different overlayer and dominant Co crystal phase; fcc (square) and hcp (hexagon).

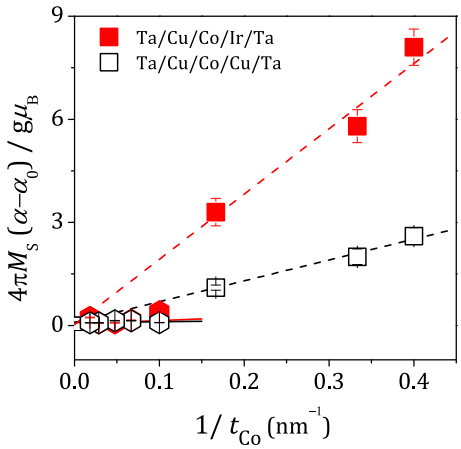

FIG. 4 (color online). The gradient of the inverse Co thickness dependence of $4\pi M_S(\alpha-\alpha_0)/g\mu_B$ directly yields spin-mixing conductances for Cu- and Ir-overlayered films with dominant fcc-Co (square) and hcp-Co (hexagon) crystal phases. The solid and dashed lines are linear fits to the hcp(0001)- and fcc(111)-dominated structures, respectively.

shows not only the expected dependence on overlayer material, but, more surprisingly, also a strong dependence on the crystal phase of the Co film directly below the interface.

This simple analysis cannot include thickness dependence of the Landé g factor, as is shown in Fig. 2(b). With knowledge of the bulk damping parameter, the gradient of the inverse Co thickness dependence of a quantity $4\pi M_S(\alpha-\alpha_0)/g\mu_B$ gives $g_{\uparrow\downarrow}^{T,\mathrm{eff}}$ directly. This is plotted in Fig. 4, using the α_0 values extracted for each film series from the data in Fig. 3. The values for $g_{\uparrow\downarrow}^{T,\mathrm{eff}}$ found from Fig. 4 relate to parallel dissipation of angular momentum in both underlayers and overlayers.

To extract the individual effective spin-mixing conductances for each Co/NM interface, note that the thinnest Co films with Cu overlayers are symmetric, with structure Ta/Cu/fcc(111)-Co/fcc(111)-Co/Cu/Ta; from this symmetric structure, the $g_{\uparrow\downarrow}^{\mathrm{eff}}$ for a single fcc(111)-Co/Cu interface can be extracted as half that found for the full structure [13]. As the lower Co interface in all samples has this exact Ta/Cu/fcc(111)-Co structure, the $g_{\uparrow\downarrow}^{\mathrm{eff}}$ for the various other Co/NM overlayer combinations can then be similarly extracted, noting that the upper Co interface of the remaining three sets of structures are composed of hcp(0001)-Co/Cu/Ta, fcc(111)-Co/Ir/Ta, and hcp(0001)-Co/Ir/Ta. The values of $g_{\uparrow\downarrow}^{\mathrm{eff}}$ for each Co/NM interface combination are given in Table I, with literature values for some similar systems quoted for comparison. Systems containing Pt have higher $g_{\uparrow\downarrow}^{\mathrm{eff}}$ than found here with Ir, as expected due to stronger SOI in Pt.

The key result of this Letter is that, for both Co/Ir and Co/Cu interfaces, the effective interfacial spin-mixing conductance depends strongly on subtle details of the local crystal structure of the Co layer directly adjacent to the interface; $g_{\uparrow\downarrow}^{\mathrm{eff}}$ for fcc(111)-Co/Ir is ~15 times that for hcp(0001)-Co/Ir, and $g_{\uparrow\downarrow}^{\mathrm{eff}}$ for fcc(111)-Co/Cu is ~4 times that for hcp(0001)x-Co/Cu.

This is incompatible with the model of Chen and Zhang [1], which requires strong (Rashba) SOI; that fcc(111)-Co/Cu has greater $g_{\uparrow\downarrow}^{\mathrm{eff}}$ than hcp(0001)-Co/Ir suggests spin memory loss due to interfacial SOI is not the dominant mechanism.

The only notable difference between hcp and fcc phases is that the atomic layer-stacking sequence within the Co film differs moving away from the interface. Considering the final atomic plane of Co to be the A lattice plane, the crystal structure in the vicinity of the interface may appear for fcc(111)-Co as $ABCA$/fcc(111)-NM, whereas for hcp(0001)-Co it would appear $BABA$/fcc(111)-NM. Because of the different atomic-scale arrangement, the electronic structure in the vicinity of the interface should differ between these two structures, which may result in differences in the effective specific interface spin resistance R^* and/or spin memory loss δ.

An enhancement in $g_{\uparrow\downarrow}^{\mathrm{eff}}$ with fcc(111)-Co over that for hcp(0001)-Co suggests that (i) R^* is smaller for the fcc(111)-Co/NM interface than for the hcp(0001)-Co/NM interface—spin current is more easily able to enter NM from fcc(111)-Co, (ii) δ is larger for the fcc(111)-Co/NM interface than for the hcp(0001)-Co/NM interface—spin-flip scattering is enhanced at the FM-NM interface with fcc(111)-Co, or (iii) a combination of these factors. Increased spin memory loss, larger δ, is primarily attributed to interfacial intermixing between FM and NM [3]; from x-ray reflectivity (not shown), no evidence is found for increased intermixing for fcc(111)-Co/NM in comparison to hcp(0001)-Co/NM films, suggesting that the effective specific interface spin

resistance R^* plays the dominant role. It is plausible that this effect is dominated by R^* as the electronic structure differs more across hcp(0001)-Co/fcc(111)-NM interfaces than across fcc(111)-Co/fcc(111)-NM interfaces.

In summary, the magnetization dynamics under ferromagnetic resonance in designed polycrystalline cobalt thin-film multilayers, overlayered with copper or iridium, was studied. Thickness-dependent evolution was observed in the magnetic properties associated with spin pumping and with microstructural changes in the cobalt layers. Consistently accounting for these factors enables access to the effective spin-mixing conductance of individual cobalt-copper and cobalt-iridium interfaces, where the cobalt layers have either fcc(111) or hcp(0001) structure. Interfacial spin mixing is significantly enhanced in structures where both the cobalt and overlayers have fcc(111) structure in comparison to those where the cobalt layer has hcp(0001) structure at the interface. These changes can be accounted for by considering extended models of interfacial spin mixing, suggesting differences in the effective specific interface spin resistance rather than interfacial spin memory loss. The dramatic influence on spin mixing due to the local microstructure in the vicinity of the interface may contribute to the spectrum of values obtained for spin-Hall angles and spin-diffusion lengths measured using a diverse range of experimental approaches.

The authors acknowledge support from EPSRC Grant Refs. EP/L000121/1 and EP/H003487/1, the Royal Society, and EU Grant No. 214499 NAMASTE, and thank M. Wang, A. W. Rushforth and B. L. Gallagher for assistance with film preparation, and C. J. Kinane for XRD at ISIS STFC R53 Materials Characterization Lab. Work at IFIMUP was supported by Portuguese Foundation of Science and Technology (FCT) through the projects EXPL/IF/00981/2013 and PTDC/FIS/120055/2010, "Investigator FCT" program (G.N.K.) and grant SFRH/BPD/63305/2009 (S. A. B.). M. T. is grateful for a scholarship from the Republic of Turkey, Ministry of National Education.

*mustafa.tokac@durham.ac.uk
†a.t.hindmarch@durham.ac.uk

[1] K. Chen and S. Zhang, Phys. Rev. Lett. **114**, 126602 (2015).
[2] Y. Liu, Z. Yuan, R. J. H. Wesselink, A. A. Starikov, and P. J. Kelly, Phys. Rev. Lett. **113**, 207202 (2014).
[3] J.-C. Rojas-Sánchez, N. Reyren, P. Laczkowski, W. Savero, J.-P. Attané, C. Deranlot, M. Jamet, J.-M. George, L. Vila, and H. Jaffrès, Phys. Rev. Lett. **112**, 106602 (2014).
[4] C. Ciccarelli, K. M. D. Hals, A. Irvine, V. Novak, Y. Tserkovnyak, H. Kurebayashi, A. Brataas, and A. Ferguson, Nat. Nano. **10**, 50 (2015).
[5] A. Kirihara, K.-i. Uchida, Y. Kajiwara, M. Ishida, Y. Nakamura, T. Manako, E. Saitoh, and S. Yorozu, Nat. Mater. **11**, 686 (2012).
[6] D. Kikuchi, M. Ishida, K. Uchida, Z. Qiu, T. Murakami, and E. Saitoh, Appl. Phys. Lett. **106**, 082401 (2015).
[7] S. S. P. Parkin, M. Hayashi, and L. Thomas, Science **320**, 190 (2008).
[8] J.-M. Hu, Z. Li, L.-Q. Chen, and C.-W. Nan, Nat. Commun. **2**, 553 (2011).
[9] M. Isasa, A. Bedoya-Pinto, S. Vélez, F. Golmar, F. Sánchez, L. E. Hueso, J. Fontcuberta, and F. Casanova, Appl. Phys. Lett. **105**, 142402 (2014).
[10] A. Brataas, Y. Tserkovnyak, G. E. W. Bauer, and B. I. Halperin, Phys. Rev. B **66**, 060404 (2002).
[11] S. Mizukami, Y. Ando, and T. Miyazaki, Phys. Rev. B **66**, 104413 (2002).
[12] Y. Tserkovnyak, A. Brataas, and G. Bauer, Phys. Rev. Lett. **88**, 117601 (2002).
[13] Y. Tserkovnyak, A. Brataas, G. E. W. Bauer, and B. I. Halperin, Rev. Mod. Phys. **77**, 1375 (2005).
[14] S. Mizukami, Y. Ando, and T. Miyazaki, J. Magn. Magn. Mater. **226–230**, 1640 (2001).
[15] M. Bjorck and G. Andersson, J. Appl. Crystallogr. **40**, 1174 (2007).
[16] S. S. Kalarickal, P. Krivosik, M. Wu, C. E. Patton, M. L. Schneider, P. Kabos, T. J. Silva, and J. P. Nibarger, J. Appl. Phys. **99**, 093909 (2006).
[17] C. Kittel, Phys. Rev. **73**, 155 (1948).
[18] For hcp(0001) cobalt there is also a weak volume perpendicular magnetic anisotropy. In FMR analysis this is assumed to be negligible as it is not possible to separate this term from M_S; this convention is followed to allow literature comparison.
[19] A. Hrabec, N. A. Porter, A. Wells, M. J. Benitez, G. Burnell, S. McVitie, D. McGrouther, T. A. Moore, and C. H. Marrows, Phys. Rev. B **90**, 020402 (2014).
[20] C. H. Lee, H. He, F. J. Lamelas, W. Vavra, C. Uher, and R. Clarke, Phys. Rev. B **42**, 1066 (1990).
[21] J.-M. Beaujour, J. Lee, A. Kent, K. Krycka, and C.-C. Kao, Phys. Rev. B **74**, 214405 (2006); J.-M. Beaujour, W. Chen, A. Kent, and J. Z. Sun, arXiv:cond-mat/0509036v1.
[22] K. Nagano, K. Tobari, M. Ohtake, and M. Futamoto, J. Phys. Conf. Ser. **303**, 012014 (2011).
[23] A. Ghosh, J. F. Sierra, S. Auffret, U. Ebels, and W. E. Bailey, Appl. Phys. Lett. **98**, 052508 (2011).
[24] J. Pelzl, R. Meckenstock, D. Spoddig, F. Schreiber, J. Pflaum, and Z. Frait, J. Phys. Condens. Matter **15**, S451 (2003).
[25] A. M. Shukh, D. H. Shin, and H. Hoffmann, J. Appl. Phys. **76**, 6507 (1994).
[26] H. Yanagihara, E. Kita, and M. B. Salamon, Phys. Rev. B **60**, 12957 (1999).
[27] R. Clarke, D. Barlett, F. Tsui, B. Chen, and C. Uher, J. Appl. Phys. **75**, 6174 (1994).
[28] See Supplemental Material at http://link.aps.org/supplemental/10.1103/PhysRevLett.115.056601 for discussion of inhomogeneous line broadening.
[29] E. Barati, M. Cinal, D. M. Edwards, and A. Umerski, Phys. Rev. B **90**, 014420 (2014).
[30] T. Devolder, P.-H. Ducrot, J.-P. Adam, I. Barisic, N. Vernier, J.-V. Kim, B. Ockert, and D. Ravelosona, Appl. Phys. Lett. **102**, 022407 (2013).